Chemical Engineering Journal Advances 20 (2024) 100679

Contents lists available at ScienceDirect

Chemical Engineering Journal Advances

journal homepage: www.sciencedirect.com/journal/chemical-engineering-journal-advances

Fabrication and characterization of UV-curable thiol-functionalized siloxane elastomers with enhanced adhesion for flexible substrates

Young-Hun Kim [a,b], Jongwon Kim [c], Jeong Ju Baek [a], Ki Cheol Chang [a], Baek Soo Park [a], Geun Yeol Bae [d], Won-Gun Koh [b,*], Gyojic Shin [a,*]

[a] Green and Sustainable Materials R&D Department Research Institute of Clean Manufacturing System, Korea Institute of Industrials Technology (KITECH), Yangdaegiro-gil 89, Ipjang-myeon, Cheonan-si 31056, South Korea
[b] Department of Chemical and Biomolecular Engineering, Yonsei University, Yonsei-ro 50, Seodaemun-gu, Seoul 03722, South Korea
[c] ThreeZeroE Co., Ltd. 362, Ori-ro, Gwangmyeong-si, Gyeonggi-do 14327, South Korea
[d] Department of Materials Design Engineering, Kumoh National Institute of Technology, Gumi 39177, South Korea

ARTICLE INFO

Keywords:
PDMS
Photocurable siloxane
Substrate adhesion
Elastomers
Flexible substrate

ABSTRACT

The rapid advancement of flexible and wearable devices has increased the demand for substrate materials with excellent elasticity, biocompatibility, and transparency. Polydimethylsiloxane (PDMS) is widely used in these applications due to its advantageous properties. However, its inherently low surface energy limits its adhesion in high-stretchability contexts. To address this issue, various surface modification techniques have been developed, but these methods often alter the intrinsic properties of PDMS or introduce complexities in the manufacturing process. This study proposes elastomers based on ultraviolet (UV)-curable siloxane resins, which retain outstanding flexibility and transparency while significantly enhancing adhesion properties. UV-curable siloxanes were synthesized to prepare elastomers that were evaluated for their mechanical, thermal, and surface properties in comparison with PDMS. Results indicate that the prepared elastomers can be rapidly cured under UV exposure, achieving storage moduli 6 and 37 times higher than those of PDMS at 25 °C and 100 °C, respectively. Furthermore, thermal conductivity improved by 60 %, and the coefficient of thermal expansion was reduced by 26 %, demonstrating superior mechanical stability across diverse conditions. Adhesion properties were also markedly enhanced, as shown by peel-test adhesion strength that was 7 times greater than that of conventional PDMS.

1. Introduction

Recent advances in the electrical and medical industries have driven increased interest in flexible and wearable devices, with a particular focus on materials that can serve as substrates for these applications [1,2]. A material suitable for wearable, flexible, or stretchable applications must possess key properties such as high flexibility, durability, biocompatibility, and the ability to maintain functionality under mechanical deformation [3–5]. Commonly used materials for these substrates include polyimide (PI) [6], polyethylene terephthalate (PET) [7], and polydimethylsiloxane (PDMS) [8]. Although PI and PET are extensively used in flexible electronics, their low elasticity limits their use in applications requiring high stretchability [9,10]. In contrast, PDMS exhibits superior mechanical elasticity, biocompatibility, and transparency, making it suitable as a stretchable substrate [11]. PDMS is extensively used in various scientific and engineering applications because of its flexibility, excellent stretchability, and ease of fabrication [12,13]. It is particularly favored for stretchable substrates because of its low cost and ability to support complex designs, such as microfluidic devices, wearable electronics, and sensors [14–16]. However, despite its advantageous properties, PDMS has an inherently low surface energy, resulting in poor adhesion with most metals and active materials [17,18]. This weak adhesion is a significant limitation in applications where PDMS-based devices are subjected to repeated mechanical stress, potentially leading to delamination or failure [19–21]. To tackle these adhesion challenges, several surface modification techniques have been proposed [22,23], including plasma treatment [24], ultraviolet (UV)-ozone treatment [25], and the use of silane coupling agents [26]. These methods chemically modify or oxidize PDMS surfaces to increase their surface energies and bonding strength with other materials. Other

* Corresponding authors.
E-mail addresses: wongun@yonsei.ac.kr (W.-G. Koh), gyshin@kitech.re.kr (G. Shin).

https://doi.org/10.1016/j.ceja.2024.100679

Available online 9 November 2024

strategies involve using intermediate adhesion layers, such as polydopamine coatings [27], which enhance adhesion by forming strong bonds with various materials. In addition, physically patterned PDMS surfaces [28], such as microstructured surfaces [29], increase the contact area and mechanical interlocking, thereby improving adhesion [30]. Although these methods have shown promise, they present challenges, including the need for precise control over processing parameters, potential changes in the mechanical and optical properties of PDMS, and scalability issues for large-area applications [31–36]. Therefore, further research is required to develop more reliable, scalable, and cost-effective strategies to enhance PDMS adhesion without compromising its desirable properties. Due to these challenges, research has been conducted on alternative materials that can maintain the advantages of PDMS while overcoming its limitations [37–40]. Recent advances in the development of photopolymerizable silicones have demonstrated their promising potential in this context [41]. Unlike conventional thermally cured silicones, photopolymerizable silicones can be rapidly processed under ultraviolet (UV) light, providing enhanced control over curing and adhesion properties. In addition, the ability to modify their chemical structure using various functional groups, such as thiol, methacrylate, and acrylate groups, allows for further optimization of the mechanical, thermal, and optical properties of photopolymerizable silicones [42–44]. This enhanced control enables tuning of material characteristics to meet the specific requirements of various flexible and wearable applications requiring robust mechanical and adhesive properties [45,46]. In this study, we synthesized thiol-functionalized, photopolymerizable siloxane resins containing either methyl groups or a combination of methyl and phenyl groups. Structural characterization was performed using gel permeation chromatography (GPC), Fourier transform infrared spectroscopy (FTIR), and nuclear magnetic resonance (NMR) spectroscopy. Elastomers with various formulations were prepared from the synthesized siloxanes and compared to commercial PDMS (SYLGARD-184). Characterization methods included UV spectrophotometry, contact angle goniometry, rheometry, universal testing (UTM), thermomechanical analysis (TMA), scanning electron microscopy (SEM), and laser flash analysis (LFA). Additionally, an LED array was fabricated to demonstrate the practical applicability of the high-transparency elastomer as a material for electronic devices. The results indicate that the developed elastomer is a viable alternative to conventional PDMS, particularly for applications requiring precise control over mechanical, thermal, and surface properties.

2. Experimental

2.1. Materials

A two-component kit of the commercially available silicone elastomer Sylgard 184 (Dow Corning, USA) comprising a prepolymer and curing agent with a default mixing weight ratio of 10:1 was used as the testing matrix/binder. (3-Mercaptopropyl) methyldimethoxysilane (MPMDMS, ≥95 %) was purchased from Sigma-Aldrich Co., Inc. Methoxytrimethylsilane (MTMS, ≥98 %), methoxytriphenylsilane (MTPS, ≥97 %), and ethyl phenyl(2,4,6-trimethylbenzoyl)phosphinate (TPO-L, ≥95 %) were supplied by TCI Co., Ltd. 4,4′-(Propane-2,2-diyl) bis((allyloxy)benzene) (PDBAB, ≥97 %) was supplied by Ambeed. All materials were used as received without further purification.

2.2. Synthesis of thiol-functionalized siloxane with methyl group (TFSC)

First, 1.5 g of hydrochloric acid (36.5 % aqueous solution, 41.15 mmol) was added to a 250 mL two-necked flask containing a mixture of solvents (26 g of ethanol and 6 g of distilled water) and stirred with a magnetic stirrer. Second, 10.52 g of MPMDMS (58.3 mmol) was added to the solvent mixture. The solution was then heated to 60 °C and stirred for 16 h under a nitrogen atmosphere. Next, 2 g of MTMS (19.2 mmol) and 0.15 g of hydrochloric acid (36.5 % aqueous solution, 4.12 mmol) were added, and the mixture was stirred at 40 °C for an additional 8 h under a nitrogen atmosphere. The mixture was then purified by pouring it into distilled water several times. Ethyl alcohol, water, methyl alcohol byproducts, and impurities were removed using a rotary evaporator. The resulting product was dried in a vacuum oven at 100 °C overnight to yield a transparent viscous liquid.

TFSC, a clear colorless liquid (yield: 89 %)

^{1}H NMR (300 MHz, $CDCl_3$, ppm): δ= 0.08–0.22 (m, Si–CH_3), 0.72–0.85 (s, Si–CH_2), 1.24–1.47 (m, Si–CH_2–CH_2–CH_2–SH), 1.62–1.78 (d, Si–CH_2–CH_2), and 2.47–2.67 (d, Si–CH_2–CH_2–CH_2); ^{13}C NMR (100.62 MHz, $CDCl_3$, ppm): δ= 1.37 (Si–CH_3), 12.18 (Si–CH_2), and 26.76 (Si–CH_2–CH_2–CH_2–SH); ^{29}Si NMR (99 MHz, $CDCl_3$, ppm): δ= 3.68 (M), -20.8 – -23.1 ($R_2Si(OSi)_2$) [D_2].

2.3. Synthesis of thiol-functionalized siloxane with methyl and phenyl groups (TFSCP)

First, 1.5 g of hydrochloric acid (36.5 % aqueous solution, 41.15 mmol) was added to a 250 mL two-necked flask containing a solvent mixture of ethanol (26 g) and distilled water (6 g) and stirred with a magnetic stirrer. Next, 10.52 g of MPMDMS (58.3 mmol) was added to the solvent mixture. The solution was heated to 60 °C and stirred for 16 h under a nitrogen atmosphere. Next, 0.72 g of MTPS (2.48 mmol) and 0.15 g of hydrochloric acid (36.5 % aqueous solution, 4.12 mmol) were added, and the mixture was stirred at 40 °C for an additional 8 h under a nitrogen atmosphere. After the reaction, the mixture was purified by pouring it into distilled water several times. Ethyl alcohol, water, methyl alcohol byproducts, and impurities were removed using a rotary evaporator. The final product was dried in a vacuum oven at 100 °C overnight, yielding a transparent viscous liquid. The syntheses of TFSC and TFSCP are illustrated in Scheme 1.

TFSCP, a clear colorless liquid (yield: 82 %)

^{1}H NMR (300 MHz, $CDCl_3$, ppm):): δ= 0.08–0.22 (m, Si–CH_3), δ= 0.72–0.87 (s, Si–CH_2), 1.25–1.55 (m, Si–CH_2–CH_2–CH_2–SH), 1.62–1.81 (d, Si–CH_2–CH_2), 2.44–2.67 (d, Si–CH_2–CH_2–CH_2), and 7.26–7.68(m, Si–PH). ^{13}C NMR (100.62 MHz, $CDCl_3$, ppm): δ= 1.37 (Si–CH_3), 11.62 (Si–CH_2), 27.29 (Si–CH_2–CH_2–CH_2–SH), 127.62 (Ortho-C), and 131.12 (Para-C), 135.08 (Meta-C).; ^{29}Si NMR (99 MHz, $CDCl_3$, ppm): δ= 2.46 (M), -20.3 – -22.8 ($R_2Si(OSi)_2$) [D_2].

2.4. Preparation of elastomers [PDBAB-TFS-CH_3 (61:38), PDBAB-TFS-CH_3 (48:51), pdbab-tfs-ch_3-PH (61:38), and pdbab-tfs-ch_3-PH (48:51)]

To prepare the elastomers, the synthesized siloxanes (TFSC and TFSCP) and resin (PDBAB) were added to a UV vial, followed by the addition of a photoinitiator (TPO-L). The mixture was then stirred in a Thinky mixer at 1500 rpm for 20 min. After mixing, the resulting mixture was poured into an aluminum (Al) mold and cured. Subsequently, the mixture was exposed to 365 nm UV light-emitting diode (LED) light for 3 min at room temperature. For the SYLGARD-184 elastomer, a prepolymer and curing agent were mixed in a 10:1 wt ratio in a vial. The mixture was then stirred in a Thinky mixer at 1500 rpm for 20 min, poured into an Al mold, and cured at 60 °C for 8 h in an oven. The details of the elastomer formulations and their abbreviations are presented in Table 1. Scheme 2 shows the structural formulas of elastomers PTC and PTCP, synthesized via photopolymerization.

2.5. Preparation of flexible substrate LED arrays

The fabrication process for a flexible LED array substrate begins with the preparation and curing of the substrate material. After curing, a thin copper (Cu) layer is transferred onto the substrate surface under heat and pressure. A photoresist layer is then applied to the Cu layer and soft-baked to prepare it for the subsequent patterning steps. Laser patterning is used to precisely generate desired features on the photoresist-covered

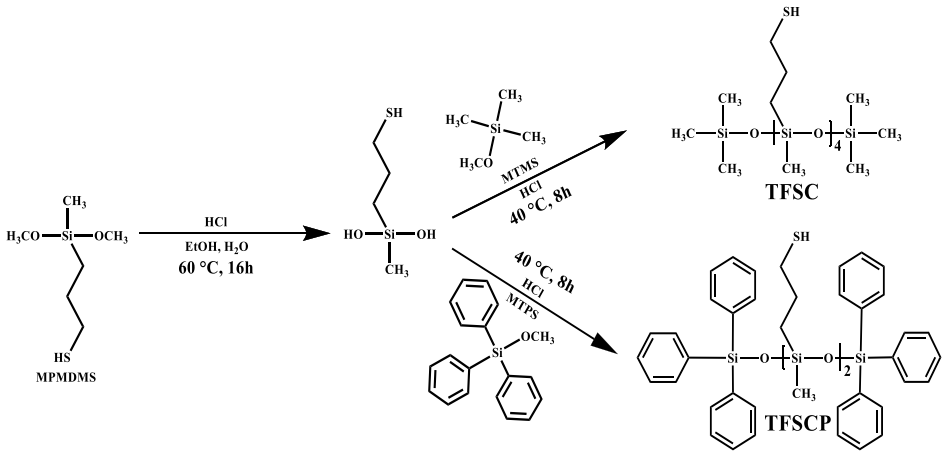

Scheme 1. Synthesis schemes for TFSC and TFSCP.

Table 1
Elastomer compositions used in this study: Formulations and abbreviations.

Elastomers	Abbreviation	Formulation (wt%)			
		PDBAB	TFSC	TFSCP	TPO-L
SYLGARD-184	**PDMS**	-	-	-	-
PDBAB-TFS-CH_3 (61:38)	**PTC-38**	61	38	-	1
PDBAB-TFS-CH_3 (48:51)	**PTC-51**	48	51	-	1
PDBAB-TFS-CH_3-PH (61:38)	**PTCP-38**	61	-	38	1
PDBAB-TFS-CH_3-PH (48:51)	**PTCP-51**	48	-	51	1

Cu layer. Following laser patterning, the exposed regions of the Cu layer are etched using a chemical etchant, leaving behind only the intended patterns. The remaining photoresist parts were removed by rinsing the substrate with an appropriate solvent, such as acetone, to clean the substrate and reveal the patterned Cu layer. Finally, LEDs were carefully soldered onto the predefined contact pads on the patterned Cu layer, thereby completing the fabrication of the flexible LED array. A schematic of the process is presented in Fig. 1.

2.6. Characterization of TFSC and TFSCP

The structural analysis of TFSC and TFSCP was performed using a Spectrum-400 FTIR spectrometer (Perkin Elmer). The samples (10 μm

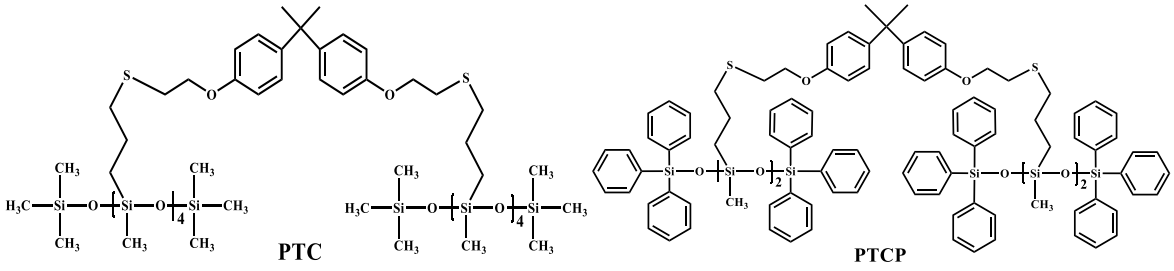

Scheme 2. Structural formula of photopolymerization-produced elastomer: PTC and PTCP.

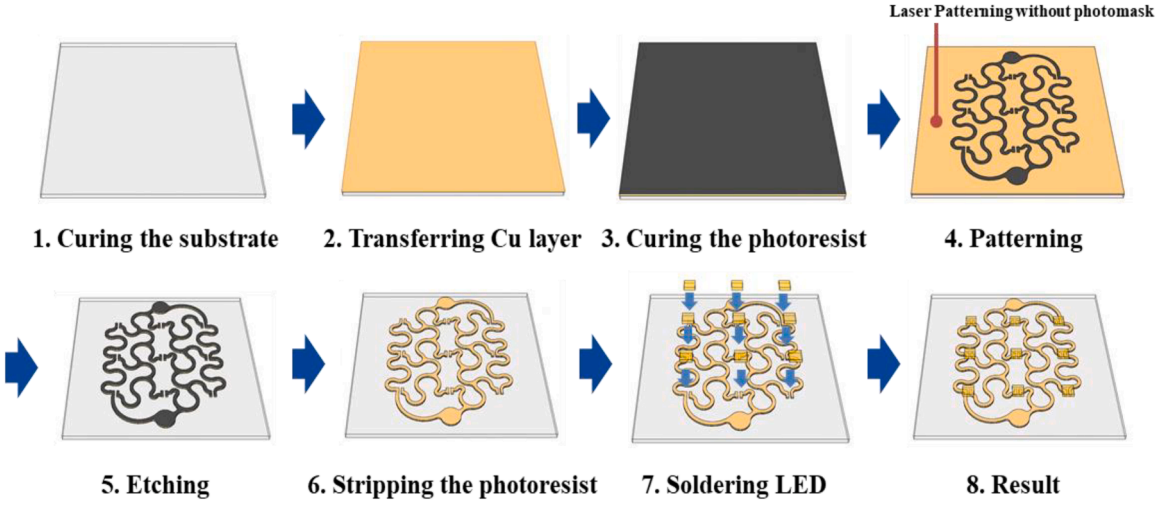

Fig. 1. Schematic of the fabrication process of LED array on flexible substrate.

thick) were applied to attenuated total reflection crystals by dropping them at room temperature. Each spectrum was obtained from 100 scans within a wavenumber range of 650–4000 cm^{-1} and was processed by reducing CO_2 interference, removing noise, and fitting the baseline. For further characterization, ^{1}H, ^{13}C, and ^{29}Si NMR spectra were recorded using a 300 MHz NMR spectrometer (Bruker, Avance 300) with $CDCl_3$ as the solvent at room temperature. The molecular weights of TFS-CH_3 and TFS-CH_3-PH were evaluated using size exclusion chromatography on an EcoSEC HLC-8320 GPC system (TOSOH Corporation). A 0.15 % (w/v) solution of each compound in tetrahydrofuran (THF) was injected into the system. Separation was performed on a series of columns, including Guard Super MP (HZ)-M+2 and TSK Gel Super-multipore HZ-M (150 mm × 4.6 mm, 3 μm), with high-performance liquid chromatography-grade THF as the mobile phase flowing at 0.45 ml/min. The column was maintained at 40 °C. The GPC system was calibrated using polystyrene standards with molecular weights ranging from 580 Da to 660,500 Da

2.7. Characterization of PDMS and new elastomers

The transmittance of the elastomers was measured using a UV spectrophotometer (UV-3600, Shimadzu, Japan). The coefficient of thermal expansion (CTE) of the elastomers was tested using TMA (HITACHI SS7300) in the temperature range of 0–200 °C at a heating rate of 5 °C/min and a preload force of 0.01 N. Thermal conductivity was measured using the LFA method by calculating thermal diffusivity. SEM analysis was performed using an NNS-450 (FEI Hong Kong Company). A UTM 5567 model (Instron, USA) was used to measure the tensile strength of the elastomer blends according to ASTM D638. Tensile tests were conducted at 10 mm/min; 10 tests were conducted for each specimen, and the mean value was used. The shear modulus was measured using a rotational rheometer (Discovery HR-10, USA) with a parallel plate geometry (diameter 20 mm, gap 1 mm) through a time sweep test. The surface characteristics of PDMS and the prepared elastomers were investigated by measuring the static contact angles with water. These measurements were performed at room temperature using the sessile drop method on a contact angle goniometer (Phoenix 300, Surface Electro Optics, Korea). The surface energy was calculated from the contact angle values using software provided by the equipment manufacturer, and the Girifalco–Good–Fowkes–Young (GGFY) method was applied. E-beam deposition was performed at approximately 0.3 Å/s, with a 5 nm Cr layer and 100 nm Au layer deposited sequentially. The adhesion strength was measured using a 180° peel test in accordance with the ASTM D903 standard. The test was conducted with an UTM-5969 model (Instron, USA) at a constant speed of 5 mm/min. To prevent elongation of the test sample, the study materials, including PDMS, were applied onto a 0.2 mm thick PET film with a layer thickness of 0.5 mm. After the adhesive layer was allowed to air-dry, the test specimens were prepared in dimensions of 220 × 25 × 1 mm^3. The peel test was performed 1 day after bonding, and to ensure accuracy, the same test was repeated on a minimum of 6 samples.

3. Results and discussion

3.1. Structural analyses of TFSC and TFSCP

Fig. 2 presents the FTIR spectra of TFSC and TFSCP, highlighting several characteristic signals that confirm the successful synthesis of these compounds. Sharp and intense peaks at 1255 cm^{-1} are observed in both TFSC and TFSCP, corresponding to the bending vibrations of Si-CH_3 groups. Additionally, TFSCP exhibits distinct absorption signals at 1429 and 1588 cm^{-1}, attributed to C-C stretching vibrations. The C-H stretching vibrations of phenyl groups appear at 3058 cm^{-1}. A weak signal at 2558 cm^{-1} in both spectra indicates the S-H stretching mode of mercapto groups. The absorption bands at 2848 and 2958 cm^{-1} are assigned to the stretching vibrations of alkane-CH_2 and Si-CH_3 groups,

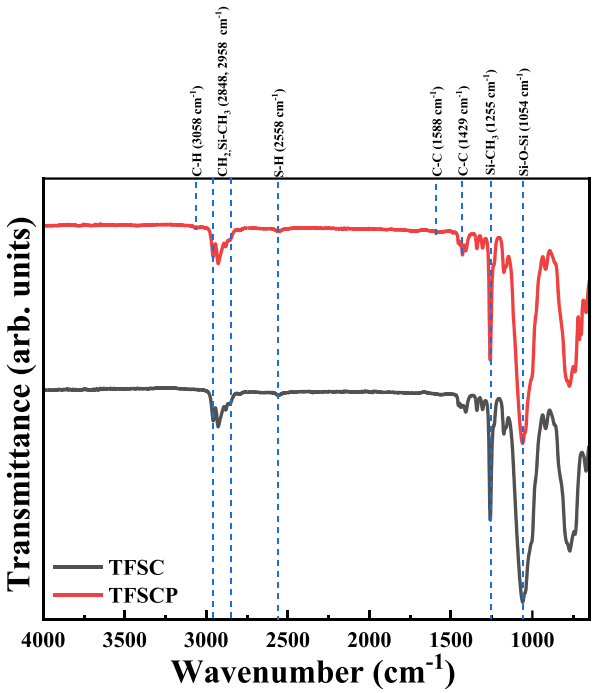

Fig. 2. FTIR spectra of the synthesized TFSC and TFSCP.

respectively. A prominent peak at 1054 cm^{-1} signifies the presence of Si–O–Si bonds within the siloxane structure.

Structural analysis of the NMR spectra for TFSC and TFSCP is provided in the Supplementary materials. Specifically, Fig. S1(a–b) present the ^{1}H NMR spectra of TFSC and TFSCP, respectively. Fig. S2(a–b) display their corresponding ^{13}C NMR spectra, and Fig. S3(a–b) show their corresponding ^{29}Si NMR spectra. In addition, gel permeation chromatography (GPC) was employed to determine the molecular weights of TFSC and TFSCP. The results, summarized in Table 2, show average molecular weights of 674 and 749 for TFSC and TFSCP, respectively, based on polystyrene calibration. The polydispersity indexes (PDIs) for TFSC and TFSCP were 1.11 and 1.17, respectively. Fig. S4 depicts the molecular weight distribution and cumulative percentage curves.

3.2. Optical characterization of PDMS and new elastomers

Fig. 3(a) compares the optical transmittance properties of PDMS and four new elastomer formulations: PTC-38, PTC-51, PTCP-38, and PTCP-51. The transmittance data show that all elastomers, including PDMS, maintained high transmittance levels above 90 % in the visible-spectrum range (400–800 nm). This finding shows that in the visible-light region, the new elastomers exhibit optical clarity nearly identical to that of PDMS. Fig. 3(b) compares the transparency of PDMS and the new elastomers, providing a confirmation for their optical clarity. However, in the UV spectrum, the new elastomers exhibit a behavior different from that of PDMS. Although PDMS exhibits a gradual decrease in transmittance as the wavelength decreases below 300 nm, the new elastomers exhibit a sharp decline to 0 % transmittance below 300 nm.

Table 2
Molecular weights of TFSC and TFSCP.

Siloxanes	Mn	Mw	Mp	Mz	Mz+1	PDI
TFSC	608	674	533	760	874	1.11
TFSCP	641	749	572	1043	1791	1.17

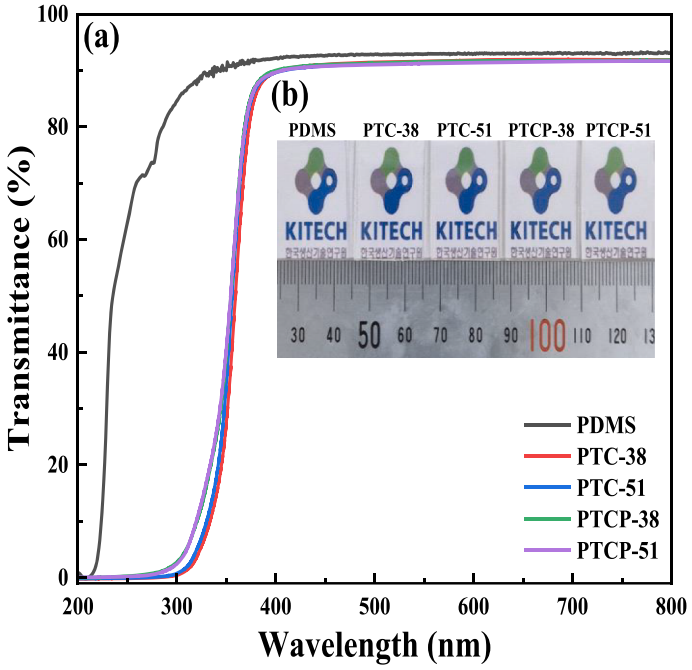

Fig. 3. (a) Optical transmittance comparison of PDMS and new elastomers, and (b) photographic images showing the visual transparency of PDMS, PTC-38, PTC-51, PTCP-38, and PTCP-51.

3.3. Characterization of surface wettability of PDMS and new elastomers

Fig. 4 shows the differences in contact angles measured for PDMS and the new elastomers, along with the surface energies calculated using the Girifalco–Good–Fowkes–Young(GGFY) method. The measured contact angles were as follows: PDMS= 104.22° ± 0.02°, PTC-38= 98.98° ± 0.02, PTC-51= 99.68° ± 0.02°, PTCP-38= 81.28° ± 0.02°, and PTCP-51= 76.29° ± 0.03° PDMS generally exhibits hydrophobicity because of its low surface energy [47], and it exhibits the lowest surface energy (10.04 mN/m). Conversely, PTCP-51, with the lowest contact angle of 76.29° ± 0.03°, exhibits the highest surface energy (27.98 mN/m). In the elastomers containing both phenyl and methyl groups, the phenyl group increased the polar component of the surface energy owing to its aromatic ring structure. This enhancement enhances the overall surface energy and improves material wettability, thereby reducing the contact angle [48]. The elemental composition (atomic %) of PDMS and the new elastomers, as determined by XPS analysis, is presented in Table S1.

3.4. Mechanical characterization of PDMS and new elastomers

As shown in Fig. 5(a–b), PDMS exhibited the lowest storage modulus (G') at both 25 °C and 100 °C. In contrast, the new elastomers exhibited significantly higher G' values than PDMS across all temperature ranges. Table 3 compares the storage moduli of PDMS and the new elastomers at 25 °C and 100 °C. As shown in Table 3, PDMS exhibited a very low storage modulus close to 0 at both 25 °C and 100 °C. Among the new

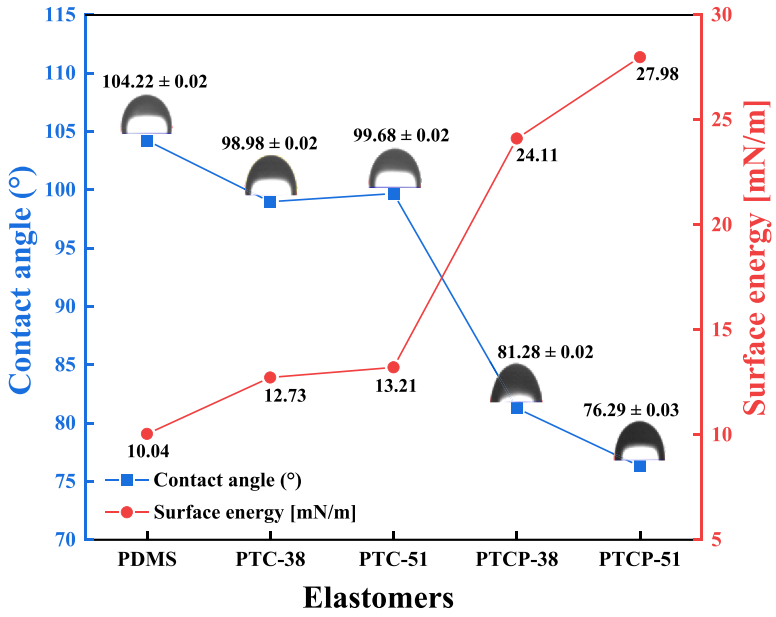

Fig. 4. Contact angles of PDMS and new elastomers, along with surface energies calculated using the GGFY Girifalco–Good–Fowkes–Young (GGFY)method.

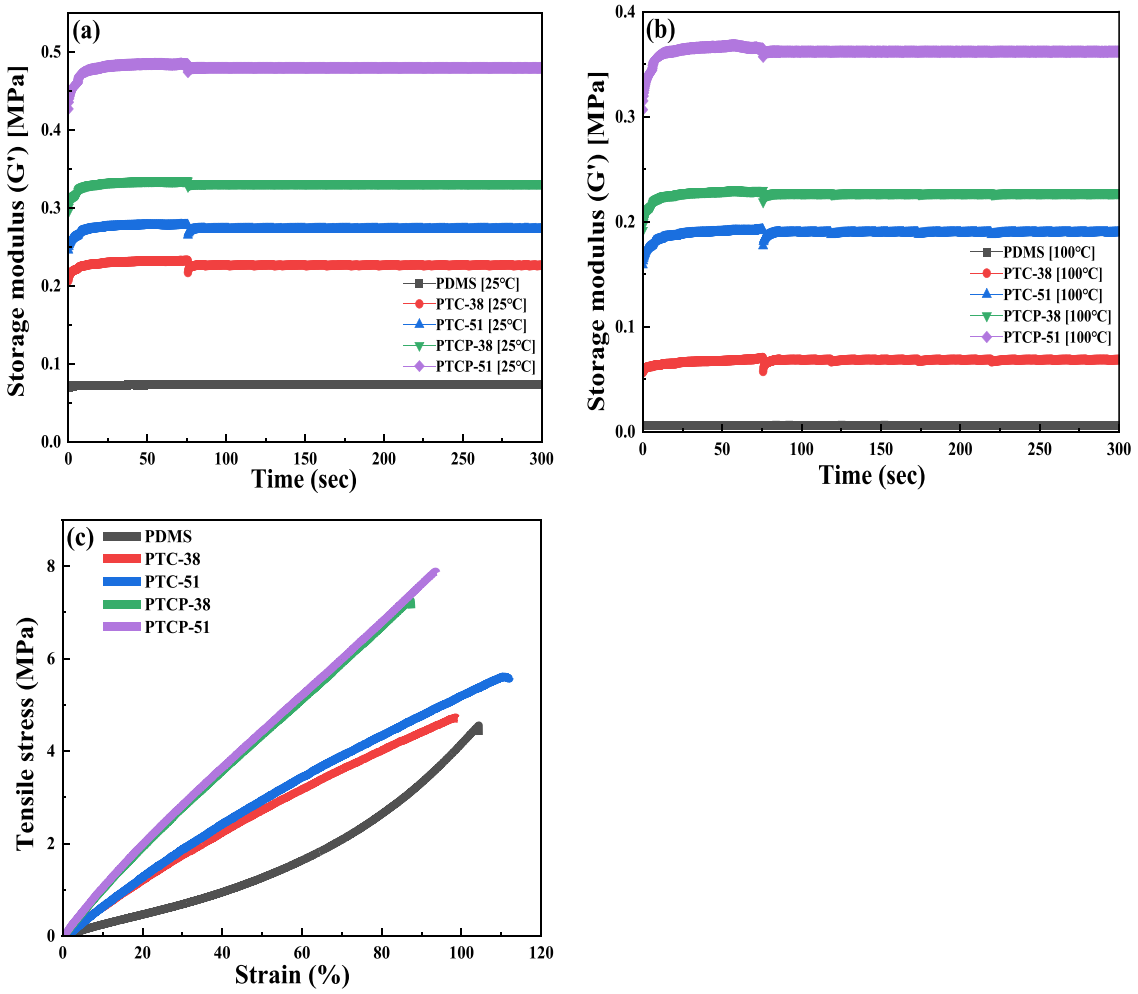

Fig. 5. Storage moduli (G') of various elastomers measured by rheometer at (a) 25 °C and (b) 100 °C, and (c) tensile stress–strain curves of the new elastomers and PDMS.

Table 3
Mechanical properties of various elastomers: storage moduli (G') at 25 °C and 100 °C and tensile stress–strain behavior.

Elastomers	25 °C Storage Modulus (G') [MPa]	100 °C Storage Modulus (G') [MPa]	Tensile stress (MPa)	Strain (%)
PDMS	≈ 0.08	≈ 0.01	4.55 ± 2.32	104.29 ± 10.31
PTC-38	≈ 0.23	≈ 0.07	4.75 ± 1.83	98.17 ± 8.98
PTC-51	≈ 0.28	≈ 0.19	5.64 ± 1.49	110.32 ± 8.01
PTCP-38	≈ 0.34	≈ 0.23	7.27 ± 0.89	87.43 ± 6.08
PTCP-51	≈ 0.49	≈ 0.37	7.91 ± 0.62	93.36 ± 4.11

elastomers, PTCP-51, which contains the highest proportion of siloxanes with both methyl and phenyl groups, exhibited the highest storage moduli at both temperatures (0.49 and 0.37 MPa at 25 °C and 100 °C, respectively). Compared with PDMS, these values correspond to approximately 6 and 37 times higher storage moduli at 25 °C and 100 °C, respectively. The findings demonstrate that the phenyl group affects the organization and packing of polymer chains, enhancing their mechanical properties through steric hindrance arising from intermolecular interactions [49,50]. In particular, the new PTCP-51 elastomer maintained a storage modulus of 0.37 MPa at 100 °C, indicating that its properties did not degrade as significantly as PDMS at elevated temperatures. Fig. 5(c) and Table 3 show the tensile stress–strain behavior of PDMS and the new elastomers with various compositions. As shown in Fig. 5(c), the tensile stress of the new elastomers increased with increasing strain up to their respective breaking points. PDMS exhibited the lowest tensile stress, reaching a maximum value of 4.55 ± 2.32 MPa at a strain of 104.29 ± 10.31 %. Among the new elastomers, PTCP-51 exhibited the highest tensile stress (7.91 ± 0.62 MPa) at a strain of 93.36 ± 4.11 %, indicating superior mechanical strength compared with PDMS. Similarly, PTCP-38 exhibited a high tensile stress (7.27 ± 0.89 MPa) at a strain of 87.43 ± 6.08 %. The combination of phenyl groups in these elastomers likely strengthens intermolecular interactions, thereby contributing to increased tensile stress [51]. The elastomers containing only methyl groups (PTC-38 and PTC-51) exhibited intermediate tensile stress values of 4.75 ± 1.83 and 5.64 ± 1.49 MPa, respectively, with strain levels of 98.17 ± 8.98 % and 110.32 ± 8.01 %.

Fig. 6(a) shows the thermal conductivity of PDMS and the new elastomers with various compositions, Fig. 6(b) shows their CTE values. As shown in Fig. 6(a), the PTCP-51 elastomer, which contains both phenyl and methyl groups, exhibits significantly improved thermal conductivity of 0.238 W/mK compared with 0.145 W/mK for PDMS. In addition, as depicted in Fig. 6(b), the CTE of PTCP-51 was the lowest among the tested materials. PDMS exhibited the highest CTE value (289.35 ppm/ °C), indicating greater thermal expansion in response to temperature changes. Conversely, PTCP-51 exhibited the lowest CTE value (213.11 ppm/ °C), suggesting reduced thermal expansion and

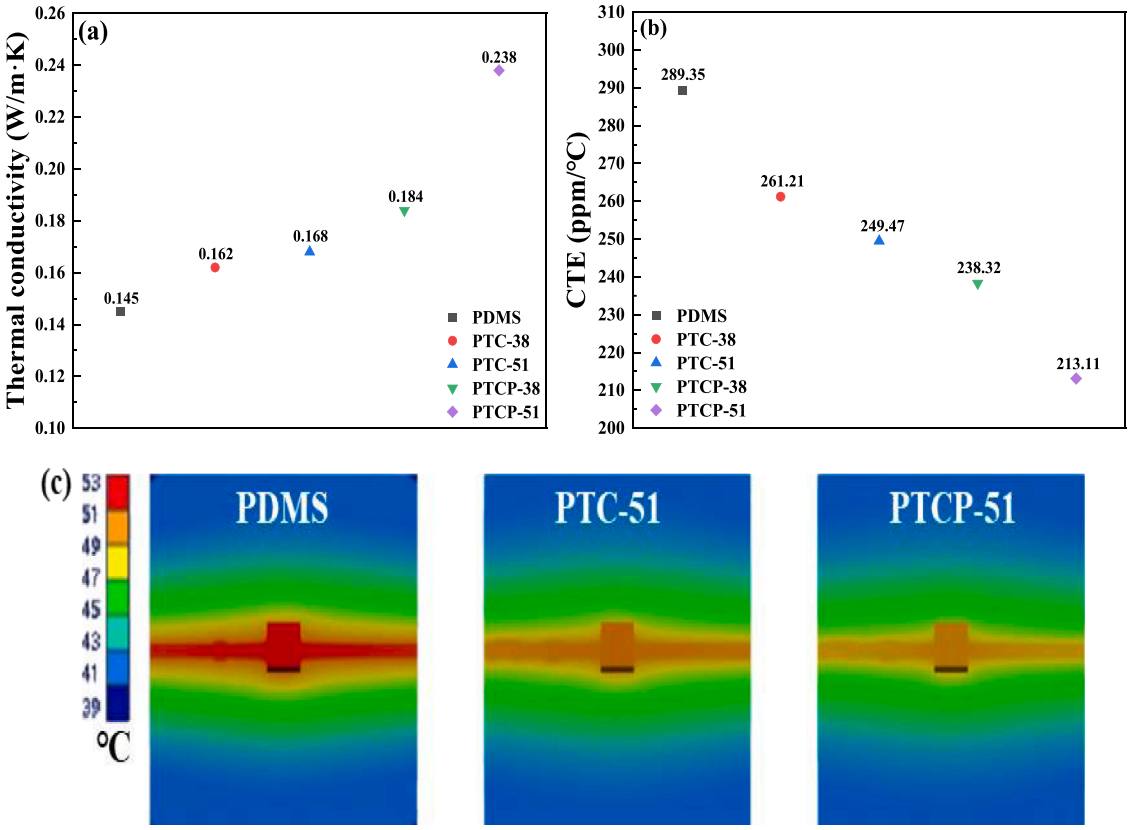

Fig. 6. Comparison of (a) thermal conductivity and (b) CTE for PDMS and new elastomers. (c) simulated thermal effects on substrates with LEDs: PDMS, PTC-51, and PTCP-51.

enhanced dimensional stability under thermal stress [52]. Compared with PDMS, the n elastomers containing both methyl and phenyl groups exhibit superior thermal stability. The π–π interactions between the phenyl groups in the elastomer matrix and the interfacial components enhance interfacial compatibility, thereby increasing thermal conductivity and reducing thermal expansion, as reflected by the lower CTE values [53,54]. Fig. 6(c) shows the effect of thermal conductivity on substrates with an attached LED, simulated based on the thermal conductivity data from Fig. 6(a). The simulation results indicate that, compared to PDMS, the PTC-51 and PTCP-51 substrates exhibit reduced thermal impact when the LED is attached, effectively dispersing heat more efficiently. This demonstrates the superior thermal management capabilities of these materials, attributed to their enhanced thermal conductivity.

3.6. Surface morphology characterization of PDMS and new elastomers

Fig. 7 shows SEM images of (a) PDMS, (b) PTC-51, and (c) PTCP-51 at various magnifications (1000x, 3000x, and 5000x) after electron beam deposition. As shown in Fig. 7(a), the SEM surface image of PDMS exhibits a rough and fractured morphology with visible cracks and voids. These surface characteristics are likely to increase the stress concentration points during thermal expansion, which is consistent with the high CTE of PDMS shown in Fig. 7(b). In contrast, the SEM image of PTC-51 in Fig. 7(b) shows a denser surface morphology than that of PDMS. Although the surface appears generally smoother, microcracks and defects remain, which may limit the performance of PTC-51 under thermal stress conditions. The SEM image of PTCP-51 in Fig.7(c) shows a smooth and uniform surface with minimal visible defects even though wrinkled structures due to thermal effects are observed.

3.7. Characterization of substrate adhesion for PDMS and new elastomers

Fig. 8(a) shows the schematic of the 180° peel test based on ASTM D 903. Fig. 8(b) presents the peel force as a function of displacement for PDMS, PTC-51, and PTCP-51 elastomers, while Fig. 8(c) compares their average peel forces. As shown in Fig. 8(b-c), the new elastomers PTC-51 (0.84 ± 0.32 N) and PTCP-51 (1.47 ± 0.49 N) demonstrate a substantial increase in peel strength compared to conventional PDMS (0.21 ± 0.12 N), with improvements of 4 times and 7 times, respectively. This significant enhancement in peel strength for PTC-51 and PTCP-51 is attributed to their ability to form stronger covalent bonds through thiol-ene reactions [55], unlike PDMS, which relies on weaker van der Waals forces [56]. The internal cross-linked network in PTC-51 and PTCP-51 improves cohesive strength, enhancing peel strength overall. In particular, PTCP-51 exhibits a peel strength that is 7 times greater, primarily due to the presence of phenyl groups, which are bulkier and more rigid than methyl groups. These phenyl groups contribute to a stiffer polymer backbone, enhancing the rigidity and cohesive strength of PTCP-51 [57]. This increased rigidity enables PTCP-51 to better resist deformation under stress, resulting in a significant improvement in peel strength.

3.8. Characterization of PDMS and new PTCP-51 in LED arrays

Fig. 9(a) shows an image of a flexible substrate prepared using the new PTCP-51 elastomer. The thermal data in Fig. 9(b) are a direct comparison of the heat dissipation performances of PDMS and PTCP-51 when used as substrates for LED arrays. As shown in the thermal image, the LED array mounted on the PTCP-51 substrate exhibited lower temperatures than the LED array on the PDMS substrate, which exhibited a higher temperature range under the same conditions. This shows that the PTCP-51 substrate exhibits better thermal management properties than PDMS because of its improved thermal conductivity and reduced

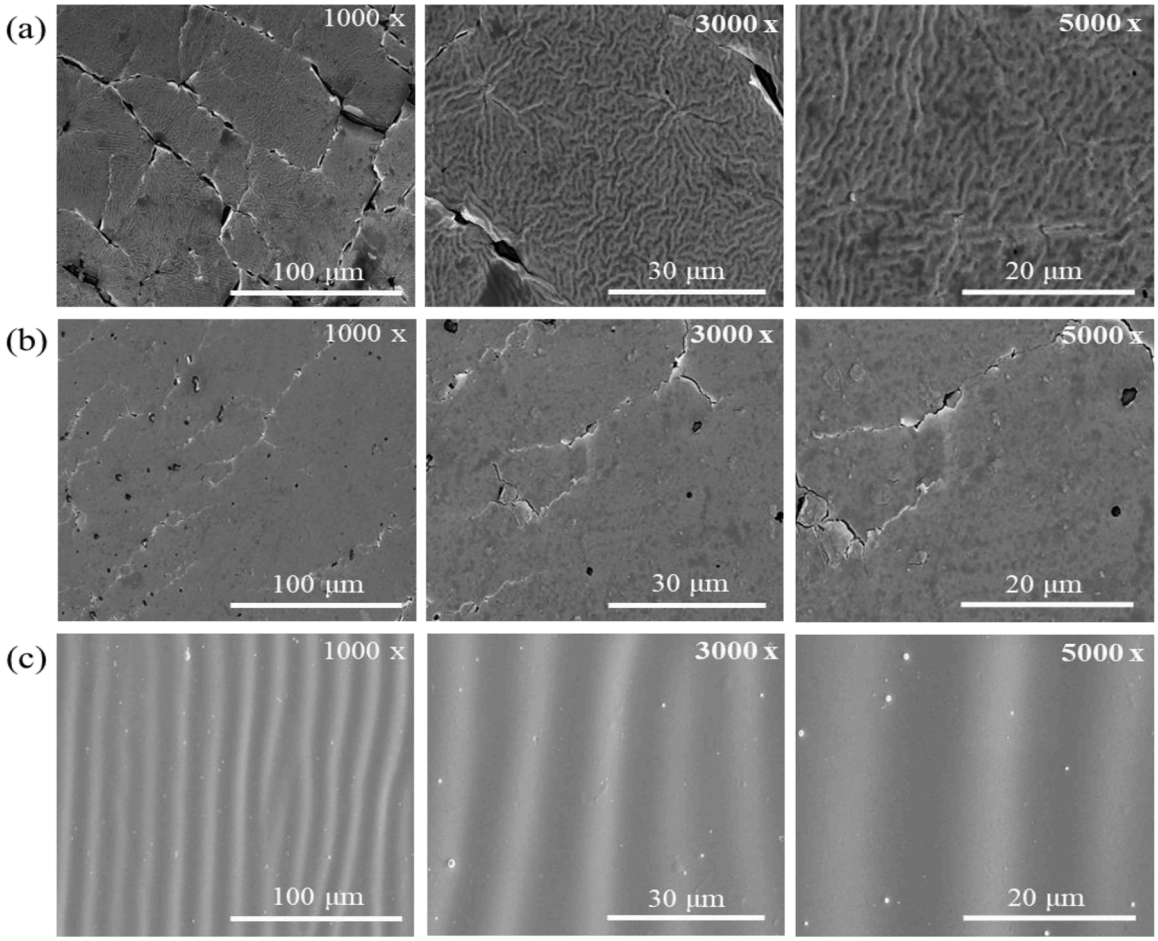

Fig. 7. Surface SEM images of (a) PDMS, (b) PTC-51, and (c) PTCP-51 derived from E-beam deposition at magnifications of 1000x, 3000x, and 5000x.

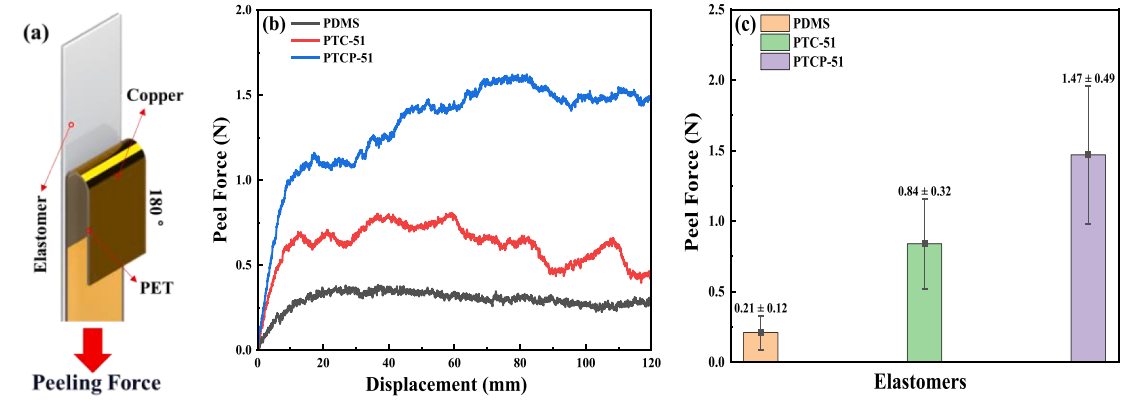

Fig. 8. (a) Schematic of the 180° peel-test for evaluating elastomer adhesion based on ASTM D 903 standard. (b) peel force as a function of displacement for PDMS, PTC-51, and PTCP-51 elastomers. (c) comparison of average peel force for PDMS, PTC-51, and PTCP-51 elastomers.

CTE, as shown in Fig. 6(a–b), which is consistent with the simulation results in Fig. 6(c). The results indicate that PTCP-51 substrates provide more efficient heat dissipation for LEDs than PDMS substrates, thereby reducing the thermal stress on LEDs. Additionally, Fig. 9(c–d) presents simulated thermal data for heat dissipation of LED arrays on PDMS and PTCP-51 substrates, respectively. The simulation results further confirm that the PTCP-51 substrate exhibits lower heat emission compared to the PDMS substrate, supporting the experimental findings.

4. Conclusion

This study successfully demonstrated that the newly developed photopolymerizable siloxane elastomers containing methyl and phenyl groups provide significant advantages over conventional PDMS in terms of mechanical and thermal properties. The new elastomers exhibited a substantial increase in storage modulus, showing values 6 times and 37 times higher than PDMS at 25 °C and 100 °C, respectively. These results indicate a marked improvement in mechanical stability across a range of thermal conditions. Additionally, the tensile strength of the new

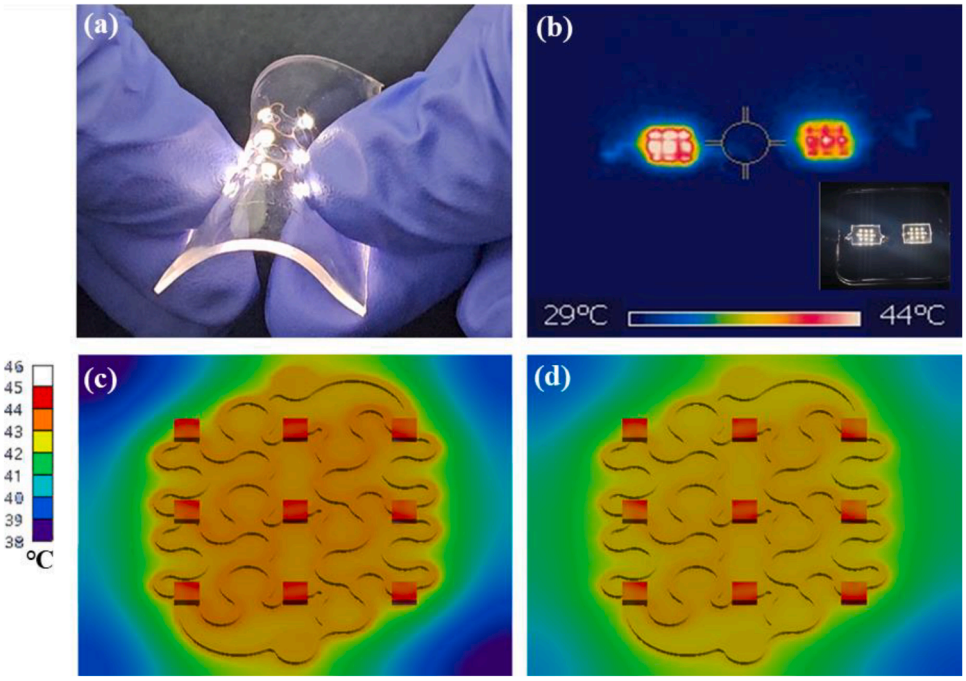

Fig. 9. (a) Image of flexible substrate prepared using new PTCP-51 elastomer. (b) thermal imaging comparison of heat dissipation for LED arrays on PTCP-51 and PDMS substrates. (c) simulated thermal data for heat dissipation of LED arrays on a PDMS substrate and (d) on a PTCP-51 substrate.

elastomers reached 7.91 ± 0.62 MPa at a strain of 93.36 ± 4.11 %, outperforming PDMS, which exhibited a tensile strength of 4.55 ± 2.32 MPa at a strain of 104.29 ± 10.31 %. This highlights the improved tensile strength of the new elastomers without significantly compromising elongation.

The thermal performance of the new elastomers was also notably superior to that of PDMS. With a thermal conductivity of 0.238 W/m•K, compared to PDMS 0.145 W/m•K, the new elastomers demonstrated enhanced heat dissipation. Furthermore, the coefficient of thermal expansion (CTE) decreased from 289.35 ppm/ °C in PDMS to 213.11 ppm/ °C in the new elastomers, indicating improved dimensional stability under thermal stress. Infrared thermal imaging data from LED arrays mounted on substrates made from the new elastomers further validated these results, showing that the LED arrays on the new elastomer substrates maintained lower temperatures than those on PDMS substrates. Adhesion properties were also markedly enhanced, with peel-test adhesion strength reaching 1.47 ± 0.49 N—7 times greater than that of conventional PDMS 0.21 ± 0.12 N.

These findings suggest that the newly developed photopolymerizable siloxane elastomers, especially those incorporating both methyl and phenyl groups, could serve as effective alternatives to PDMS. With their improved mechanical strength, higher adhesion, and superior thermal management and dimensional stability, these elastomers represent promising candidates for applications where material reliability under mechanical and thermal stress is critical.

CRediT authorship contribution statement

Young-Hun Kim: Conceptualization, Data curation, Resources, Investigation, Writing – original draft. **Jongwon Kim:** Methodology, Software, Visualization. **Jeong Ju Baek:** Investigation, Formal analysis. **Ki Cheol Chang:** Investigation, Data curation. **Baek Soo Park:** Writing – review & editing. **Geun Yeol Bae:** Writing – review & editing. **Won-Gun Koh:** Validation, Writing – review & editing. **Gyojic Shin:** Supervision.

Declaration of competing interest

The authors declare that they have no conflicting financial interests or personal relationships that could have influenced the work reported in this study.

Acknowledgments

This work was supported by the Technology Innovation Program Development Program (2001–1031) funded by the Ministry of Trade, Industry and Energy (MOTIE, Republic of Korea).

Supplementary materials

Supplementary material associated with this article can be found, in the online version, at doi:10.1016/j.ceja.2024.100679.

Data availability

Data will be made available upon request with the corresponding author's consent.

Referencess

[1] W Wu, Stretchable electronics: Functional materials, fabrication strategies and applications, Sci. Technol. Adv. Mater. 20 (2019) 187–224, https://doi.org/10.1080/14686996.2018.1549460.
[2] H Lee, Z Jiang, T Yokota, K Fukuda, S Park, T Someya, Stretchable organic optoelectronic devices: design of materials, structures, and applications, Mater. Sci. Eng. R. Rep. 146 (2021) 100631, https://doi.org/10.1016/j.mser.2021.100631.
[3] C Wang, T Yokota, T Someya, Natural biopolymer-based biocompatible conductors for stretchable bioelectronics, Chem. Rev. (2021) 1212109–1212146, https://doi.org/10.1021/acs.chemrev.0c00897.
[4] JA Rogers, T Someya, Y Huang, Materials and mechanics for stretchable electronics, Science 327 (2010) 1603–1607, https://doi.org/10.1126/science.1182383.
[5] J Onorato, V Pakhnyuk, CK Luscombe, Structure and design of polymers for durable, stretchable organic electronics, Polym. J. 49 (2017) 41–60, https://doi.org/10.1038/pj.2016.76.

[6] YY Hsu, M Gonzalez, F Bossuyt, J Vanfleteran, ID Wolf, Polyimide-enhanced stretchable interconnects: design, fabrication, and characterization, IEEe Trans. Electron. Devices 58 (2011) 2680–2688, https://doi.org/10.1109/TED.2011.2147789.
[7] X Hou, J Zhu, J Qian, X Niu, J He, J Mu, W Geng, C Xue, X Chou, Stretchable triboelectric textile composed of wavy conductive-cloth PET and patterned stretchable electrode for harvesting multivariant human motion energy, ACS. Appl. Mater. Interfaces. 10 (2018) 43661–43668, https://doi.org/10.1021/acsami.8b16267.
[8] A Larmagnac, S Eggenberger, H Janossy, J Vörös, Stretchable electronics based on Ag-PDMS composites, Sci. Rep. 4 (2014) 7254, https://doi.org/10.1038/srep07254.
[9] H Wang, Z Zhao, P Liu, X Guo, A soft and stretchable electronics using laser-induced graphene on polyimide/PDMS composite substrate, Npj. Flex. Electron. 6 (2022) 26, https://doi.org/10.1038/s41528-022-00161-z.
[10] Z Yang, W Wang, L Bi, L Chen, G Wang, G Chen, C Ye, J Pan, Wearable electronics for heating and sensing based on a multifunctional PET/silver nanowire/PDMS yarn, Nanoscale 12 (2020) 16562–16569, https://doi.org/10.1039/d0nr04023a.
[11] TQ Trung, Lee NE, Recent progress on stretchable electronic devices with intrinsically stretchable components, Adv. Mater. 29 (2017) 1603167, https://doi.org/10.1002/adma.201603167.
[12] R Seghir, S Arscott, Extended PDMS stiffness range for flexible systems, Sens. Actuat. A Phys. 230 (2015) 33–39, https://doi.org/10.1016/j.sna.2015.04.011.
[13] J Huang, Y Cai, C Xue, J Ge, H Zhao, S-H Yu, Highly stretchable, soft and sticky PDMS elastomer by solvothermal polymerization process, Nano Res. 14 (2021) 3636–3642, https://doi.org/10.1007/s12274-021-3390-3.
[14] R Ariati, F Sales, A Souza, RA Lima, J Ribeiro, Polydimethylsiloxane composites characterization and its applications: a review, Polymers. (Basel) 13 (2021) 4258, https://doi.org/10.3390/polym13234258.
[15] D Zhu, S Handschuh-Wang, X Zhou, Recent progress in fabrication and application of polydimethylsiloxane sponges, J. Mater. Chem. A 5 (2017) 16467–16497, https://doi.org/10.1039/C7TA04577H.
[16] S Li, J Zhang, J He, W Liu, YH Wang, Z Huang, H Pang, Y Chen, Functional PDMS elastomers: Bulk composites, surface engineering, and precision fabrication, Adv. Sci. 10 (2023) e2304506, https://doi.org/10.1002/advs.202304506.
[17] U Eduok, O Faye, J Szpunar, Recent developments and applications of protective silicone coatings: a review of PDMS functional materials, Prog. Org. Coat. 111 (2017) 124–163, https://doi.org/10.1016/j.porgcoat.2017.05.012.
[18] A Lamberti, M Quaglio, A Sacco, M Cocuzza, Pirri CF Surface energy tailoring of glass by contact printed PDMS, Appl. Surf. Sci. 258 (2012) 9427–9431, https://doi.org/10.1016/j.apsusc.2011.12.117.
[19] CF Chen, K Wharton, Characterization and failure mode analyses of air plasma oxidized PDMS-PDMS bonding by peel testing, RSC. Adv. 7 (2017) 1286–1289, https://doi.org/10.1039/C6RA25947B.
[20] D Torres-Alvarez, A Aguirre-Soto, Polydimethylsiloxane chemistry for the fabrication of microfluidics—perspective on its uniqueness, limitations and alternatives, Mater. Today Proc. 48 (2022) 88–95, https://doi.org/10.1016/j.matpr.2020.10.295.
[21] O Akogwu, D Kwabi, S Midturi, M Elerujab, B Babatoped, WO Soboyejoa, Large strain deformation and cracking of nano-scale gold films on PDMS substrate, Mater. Sci. Eng. B 170 (2010) 32–40, https://doi.org/10.1016/j.mseb.2010.02.023.
[22] J Zhou, DA Khodakov, AV Ellis, NH Voelcker, Surface modification for PDMS-based microfluidic devices, Electrophoresis 33 (2012) 89–104, https://doi.org/10.1002/elps.201100482.
[23] Z Almutairi, CL Ren, L Simon, Evaluation of polydimethylsiloxane (PDMS) surface modification approaches for microfluidic applications, Colloids. Surf. A Physicochem. Eng. Asp. 415 (2012) 406–412, https://doi.org/10.1016/j.colsurfa.2012.10.008.
[24] D Lee, S Yang, Surface modification of PDMS by atmospheric-pressure plasma-enhanced chemical vapor deposition and analysis of long-lasting surface hydrophilicity, Sens. Actuat. B Chem. 162 (2012) 425–434, https://doi.org/10.1016/j.snb.2011.12.017.
[25] Y Berdichevsky, J Khandurina, A Guttman, YH Lo, UV/ozone modification of poly (dimethylsiloxane) microfluidic channels, Sens. Actuat. B Chem. 97 (2004) 402–408, https://doi.org/10.1016/j.snb.2003.09.022.
[26] A Shakeri, S Khan, TF Didar, Conventional and emerging strategies for the fabrication and functionalization of PDMS-based microfluidic devices, Lab. Chip. 21 (2021) 3053–3075, https://doi.org/10.1039/d1lc00288k.
[27] P Xue, Q Li, Y Li, L Sun, L Zhang, Z Xu, Y Kang, Surface modification of poly (dimethylsiloxane) with polydopamine and hyaluronic acid to enhance hemocompatibility for potential applications in medical implants or devices, ACS. Appl. Mater. Interfaces. 9 (2017) 33632–33644, https://doi.org/10.1021/acsami.7b10260.
[28] CL Gonzalez-Gallardo, A Díaz Díaz, JR Casanova-Moreno, Improving plasma bonding of PDMS to gold-patterned glass for electrochemical microfluidic applications, Microfluid Nanofluid 25 (2021) 1–11, https://doi.org/10.1007/s10404-021-02420-3.
[29] H Shahsavan, B Zhao, Conformal adhesion enhancement on biomimetic microstructured surfaces, Langmuir. 27 (2011) 7732–7742, https://doi.org/10.1021/la200893n.
[30] Q Wang, A Chen, H Gu, G Qin, J Zhang, J Xu, G Jiang, W Liu, Z Zhang, H Haung, Highly interconnected porous PDMS/CNTs sandwich sponges with anti-icing/deicing microstructured surfaces, J. Mater. Sci. 56 (2021) 11723–11735, https://doi.org/10.1007/s10853-021-06052-4.
[31] A Tony, I Badea, C Yang, Y Liu, G Wells, K Wang, R Yin, H Zhang, W Zhang, The additive manufacturing approach to polydimethylsiloxane (PDMS) microfluidic devices: Review and future directions, Polymers. (Basel) 15 (2023) 1–18, https://doi.org/10.3390/polym15081926.
[32] IE Araci, P Brisk, Recent developments in microfluidic large scale integration, Curr. Opin. Biotechnol. 25 (2014) 60–68, https://doi.org/10.1016/j.copbio.2013.08.014.
[33] M K Raj, S Chakraborty, PDMS microfluidics: a mini review, J. Appl. Polym. Sci. 137 (2020) 48958, https://doi.org/10.1002/app.48958.
[34] J Zhou, AV Ellis, NH Voelcker, Recent developments in PDMS surface modification for microfluidic devices, Electrophoresis 31 (2010) 2–16, https://doi.org/10.1002/elps.200900475.
[35] I Miranda, A Souza, P Sousa, J Ribeiro, EMS Castanheira, R Lima, G Minas, Properties and applications of PDMS for biomedical engineering: a review, J. Funct. Biomater. 13 (2021) 2, https://doi.org/10.3390/jfb13010002.
[36] T Zhu, Y Yuan, L Song, X Wei, H Xiang, X Dai, X Hua, R Liao, A PDMS coating with excellent durability for large-scale deicing, J. Mater. Res. Technol. 29 (2024) 4526–4536, https://doi.org/10.1016/j.jmrt.2024.02.177.
[37] JK Wu, KW Zheng, XC Nie, H-R Ge, Q-Y W, J-T Xu, Promoters for improved adhesion strength between addition-cured liquid silicone rubber and low-melting-point thermoplastic polyurethanes, Materials. (Basel) 15 (2022) 991, https://doi.org/10.3390/ma15030991.
[38] Y Wang, Y Ling, S Zhou, Y Chen, M Liang, H Zou, Enhanced mechanical and adhesive properties of PDMS based on novel PDMS-epoxy IPN structure, J. Polym. Res. 28 (2021) 171, https://doi.org/10.1007/s10965-021-02518-w.
[39] J Li, Y Liu, H Zhang, F Usta, Y Chen, SH Kang, W Zhou, Multifunctional architected MWCNTs/PDMS composites with high sensing and energy absorption capability inspired by ant tentacle and pomelo peel, J. Mater. Res. Technol. 24 (2023) 9045–9057, https://doi.org/10.1016/j.jmrt.2023.05.151.
[40] PP Singh, A De, A Mondal, P Maity, BB Khatua, Thermally tunable ethanol impregnated PDMS/CoZTO/SWCNT composite architecture for smart electromagnetic shielding, Chem. Eng. J. Adv. 16 (2023) 100586, https://doi.org/10.1016/j.ceja.2023.100568.
[41] B Jiang, X Shi, T Zhang, Y Huang, Recent advances in UV/thermal curing silicone polymers, Chem. Eng. J. 435 (2022) 134843, https://doi.org/10.1016/j.cej.2022.134843.
[42] M Roth, A Oesterreicher, FH Mostegel, A Moser, G Pinter, M Edler, R Piock, T Griesser, Silicon-based mercaptans: High-performance monomers for thiol-ene photopolymerization, J. Polym. Sci. Part A: Polym. Chem. 54 (2016) 418–424, https://doi.org/10.1002/pola.27792.
[43] C Ingrosso, C Esposito Corcione, R Striani, R Comparelli, M Striccoli, A Agostiano, ML Curri, M Frigione, UV-curable nanocomposite based on methacrylic-siloxane resin and surface-modified TiO2 nanocrystals, ACS. Appl. Mater. Interfaces. 7 (2015) 15494–15505, https://doi.org/10.1021/acsami.5b03731.
[44] CE Corcione, A Previderio, M Frigione, Kinetics characterization of a novel photopolymerizable siloxane-modified acrylic resin, Thermochim. Acta 509 (2010) 56–61, https://doi.org/10.1016/j.tca.2010.06.001.
[45] H Xiang, X Wang, Z Ou, G Lin, J Yin, Z Liu, L Zhang, X Liu, UV-curable, 3D printable and biocompatible silicone elastomers, Prog. Org. Coatings 137 (2019) 105372, https://doi.org/10.1016/j.porgcoat.2019.105372.
[46] J Palaganas, AC de Leon, J Mangadlao, N Palaganas, A Marl, YJ Lee, HY Lai, R Advincula, Facile preparation of photocurable siloxane composite for 3D printing, Macromol. Mater. Eng. 302 (2017) 1600477, https://doi.org/10.1002/mame.201600477.
[47] F Wang, TE Tay, Y Sun, W Liang, B Yang, Low voltage and -surface energy SWCNT/poly(dimethylsiloxane) (PDMS) nanocomposite film: Surface wettability for passive anti-icing and surface-skin heating for active deicing, Compos. Sci. Technol. 184 (2019) 107872, https://doi.org/10.1016/j.compscitech.2019.107872.
[48] N Kumar, A Jyothirmayi, KRC Soma Raju, R Subasri, Effect of functional groups (methyl, phenyl) on organic-inorganic hybrid sol-gel silica coatings on surface modified SS 316, Ceram. Int. 38 (2012) 6565–6572, https://doi.org/10.1016/j.ceramint.2012.05.040.
[49] Y-H Kim, JJ Baek, KC Chang, HS Lim, M-S Choi, W-G Koh, G Shin, Influence of thiol-functionalized polysilsesquioxane/phosphorus flame-retardant blends on the flammability and thermal, mechanical, and volatile organic compound (VOC) emission properties of epoxy resins, Polymers. (Basel) 16 (2024) 842, https://doi.org/10.3390/polym16060842.
[50] L Zhu, S Zhao, C Zhang, X Cheng, J Hoa, X Shao, C Zhou, Effects of chain structure on damping property and local dynamics of phenyl silicone rubber: Insights from experiment and molecular simulation, Polym. Test. 93 (2021) 106885, https://doi.org/10.1016/j.polymertesting.2020.106885.
[51] Z Liu, H Wang, C Zhou, The effect of phenyl content on the liquid crystal-based organosilicone elastomers with mechanical adaptability, Polymers. (Basel) 14 (2022) 903, https://doi.org/10.3390/polym14050903.
[52] JL Faust, PG Kelly, BD Jones, Roy-Mayhew JD, Effects of coefficient of thermal expansion and moisture absorption on the dimensional accuracy of carbon-reinforced 3D printed parts, Polymers. (Basel) 13 (2021) 3637, https://doi.org/10.3390/polym13213637.
[53] M Sheng, R Yang, H Gong, Y Zhang, X Lin, J Jing, Enhanced thermal conductivity and stability of boron nitride/phenyl silicone rubber composites via surface modification and grain alignment, J. Mater. Sci. 57 (2022) 5805–5824, https://doi.org/10.1007/s10853-021-06860-8.
[54] JG Um, S Habibpour, YS Jun, A Elkame, A Yu, Development of π–π interaction-induced functionalized graphene oxide on mechanical and anticorrosive properties

of reinforced polyurethane composites, Ind. Eng. Chem. Res. 59 (2020) 3617–3628, https://doi.org/10.1021/acs.iecr.9b06755.
[55] M.A Cole, C.N Bowman, Evaluation of thiol-ene click chemistry in functionalized polysiloxanes, J.Polym. Sci. A Polym. Chem 51 (2013) 1749–1757, https://doi.org/10.1002/pola.26551.
[56] V.M Gun'ko, V.V Turov, A.A Turova, T.V Krupska, P Pissis, R Leboda, J Skubiszewska-Zie˛ba, Interactions of poly(dimethylsiloxane) with nanosilica and silica gel upon cooling–heating, J. Colloid. Interface Sci. 426 (2014) 48–55, https://doi.org/10.1016/j.jcis.2014.03.055.
[57] K Kunal, C.G Robertson, S Pawlus, S.F Hahn, A.P Sokolov, Role of chemical structure in fragility of polymers: a qualitative picture, Macromolecules. 41 (2008) 7232–7238, https://doi.org/10.1021/ma801155c.